



CHORUS

This is the accepted manuscript made available via CHORUS. The article has been published as:

Relieving frustration: The case of antiferromagnetic Mn_3 molecular triangles

J. Liu, C. Koo, A. Amjad, P. L. Feng, E.-S. Choi, E. del Barco, D. N. Hendrickson, and S. Hill

Phys. Rev. B **84**, 094443 — Published 26 September 2011

DOI: [10.1103/PhysRevB.84.094443](https://doi.org/10.1103/PhysRevB.84.094443)

Relieving Frustration: the Case of Antiferromagnetic Mn_3 Molecular Triangles

J. Liu,^{1,2} C. Koo,¹ A. Amjad,³ P. L. Feng,⁴ E.-S. Choi,² E. del Barco,³ D. N. Hendrickson⁴ and
S. Hill^{*,2,5}

¹Department of Physics, University of Florida, Gainesville, FL32611

²National High Magnetic Field Laboratory, Florida State University, Tallahassee, FL32310

³Department of Physics, University of Central Florida, Orlando, Florida 32816-2385

⁴Department of Chemistry and Biochemistry, University of California, San Diego, La Jolla, CA
92093

⁵Department of Physics, Florida State University, Tallahassee, FL32310

Abstract

Recently, various triangular $[Mn^{III}]_3$ molecules have been extensively studied due to the fact that one can modulate the magnitude and the sign of the inter-ion exchange, thereby giving rise to very simple clusters that constitute some of the cleanest and best examples of so-called single-molecule magnets (SMMs). However, magnetic and electron paramagnetic resonance (EPR) characterizations of low-spin antiferromagnetic $[Mn^{III}]_3$ complexes have been problematic due to the significant spin frustration that exists for this topology. We show that this frustration is relieved in the highly distorted $[NEt_4]_3Mn_3Zn_2(salox)_3O(N_3)_8 \cdot MeOH$ molecule: susceptibility data suggest a well isolated $S = 2$ ground state; EPR spectroscopy and high-field torqueometry support this conclusion and further indicate the presence of a very significant zero-field-splitting

(zfs) separating the lowest-lying $m_S = \pm 2$ states from the excited levels within the same $S = 2$ multiplet. Remarkably, this zfs is sufficient to give rise to magnetic bistability, as evidenced through the observation of low-temperature magnetization hysteresis.

II. Introduction

Mn^{III} is frequently used as a basic component in the synthesis of single molecule-magnets (SMMs [1-3]); indeed, the vast majority of known SMMs contain Mn^{III} [4]. This is due in part to the flexibility of manganese chemistry, which facilitates the synthesis of relatively simple polynuclear clusters possessing appreciable unpaired electron counts (hence, large spin, S), and to the propensity for octahedrally coordinated Mn^{III} to undergo a Jahn-Teller (JT) distortion, resulting in significant easy-axis (Ising-type) magneto-anisotropy [5]. The triangular [Mn₃-(μ_3 -oxo)] motif seen at the core of the molecule in Fig. 1 has been extensively studied in this regard [6-19]. For a long time, it was believed that this topology would result exclusively in antiferromagnetic (AF) coupling and, hence, to a low-spin ground state. However, work over the past decade has shown that it is possible to engender ferromagnetic (FM) coupling within homovalent [Mn₃^{III}-(μ_3 -oxo)] triangles via ligand-imposed distortions to both the planarity of the core and the peripheral bridges [8,10,15,16,18]. This has resulted in some exceptional $S = 6$ SMMs [17-21]; indeed, the effective magnetization relaxation barrier for the best Mn₃ SMM is ~70% of that for Mn₁₂-acetate [3]. This motivated efforts to extend such strategies to larger molecules containing triangular [Mn₃^{III}-(μ_3 -oxo)] units, resulting in a series of FM Mn₆^{III} SMMs, which currently hold the record for both blocking temperature and anisotropy barrier for any transition metal-based SMM [22-27].

The aforementioned activities have stimulated a considerable body of experimental and theoretical work focused on a vast library of $[\text{Mn}_3^{\text{III}}-(\mu_3\text{-oxo})]$ molecules (see e.g. [17-19,28]). Of particular interest has been the interplay between isotropic ($\text{Mn}\cdots\text{Mn}$) exchange and single-ion anisotropy, with the aim of answering long-standing questions concerning strategies for increasing overall molecular anisotropy (for a review, see [19,29,30]). The Mn_3^{III} molecules are very attractive from this perspective, due to their inherent simplicity when compared to larger clusters, and due to the fact that one can controllably modulate the exchange. Spectroscopic measurements [mainly inelastic neutron scattering (INS) and electron paramagnetic resonance (EPR)] have been particularly important, with some of the FM Mn_3^{III} molecules providing perhaps the cleanest examples in the SMM literature [16,31]. However, in spite of exhaustive efforts, it has not been possible to obtain detailed spectroscopic information concerning the molecular anisotropy for any of the AF Mn_3^{III} molecules until recently [17,18,32]. This has prevented detailed comparisons between AF and FM complexes along the lines of recent work reported for Mn_6^{III} [19,27,30,33]. As we demonstrate in the present study, this can be attributed to the spin frustration inherent to AF triangular systems [34]. Of course, in the case of maximal frustration (perfect equilateral triangle), one anticipates a non-magnetic ($S = 0$) ground state for the pure Heisenberg case. However, even in cases with significant Ising-type anisotropy, the effects caused by frustration remain, leading to a considerable density of low-lying spin states and to a significant mixing between these states. These factors typically give rise to broad, content-less EPR spectra (see e.g. [17,18]).

In this article, we present detailed high-field EPR and magnetization studies of the distorted $[\text{NEt}_4]_3[\text{Mn}_3\text{Zn}_2(\text{salox})_3\text{O}(\text{N}_3)_8]\cdot\text{MeOH}$ complex (Fig. 1). We show that the distortion from a perfect equilateral geometry leads to a significant relief of the spin frustration within the

molecule, as evidenced by very clean EPR spectra. The EPR measurements identify a reasonably isolated $S = 2$ spin ground state, which possesses a very significant uniaxial molecular magneto-anisotropy, or zero-field splitting (zfs). Moreover, low temperature Hall-effect magnetometry studies reveal magnetic hysteresis—the hallmark of a SMM. This observation is consistent with the significant anisotropy deduced via EPR. In addition, high field (up to 35 T) magnetic torque measurements reveal multiple spin-crossover transitions involving excited states of higher spin value ($S > 2$). Simulations of the combined results, using a multi-spin Hamiltonian that considers the individual Mn single-ion anisotropies and the AF exchange between the ions, are in excellent agreement with the experiments.

II. Experimental

The $[\text{NEt}_4]_3[\text{Mn}_3\text{Zn}_2(\text{salox})_3\text{O}(\text{N}_3)_8]\cdot\text{MeOH}$ molecule is comprised of an approximately planar $[\text{Mn}_3^{\text{III}}-(\mu_3\text{-oxo})]^{7+}$ triangular core, as depicted in Fig. 1 [17]. Each Mn^{III} (d^4) ion has a nearly octahedral coordination geometry with an axial JT distortion (elongation). The neighboring Mn^{III} ions are coupled magnetically through the central $\mu_3\text{-oxo}$ atom, and also via peripheral oximate (Mn-N-O-Mn) bridges. The latter pathway turns out to be more relevant in terms of determining the sign of the exchange within this family of clusters [16-19]. In the present case, the oximate bridges lie close to the plane of the Mn_3 core, resulting in AF coupling. Non-magnetic Zn^{II} capping ions do not contribute directly to the magnetic moment of the molecule, but they do constrain the Mn(III) JT axes, which are almost exactly ($< 3.7^\circ$ away from) perpendicular to the plane of the Mn_3^{III} triangle. It is these near parallel JT axes that are responsible for the easy-axis (Ising-type) anisotropy of the molecule.

The $[\text{NEt}_4]_3[\text{Mn}_3\text{Zn}_2(\text{salox})_3\text{O}(\text{N}_3)_8]$ molecule (**3** in Ref. [17], hereon denoted AF Mn_3Zn_2) belongs to a wider family of complexes that have been described in considerable detail elsewhere [17]. It should be noted, however, that most of the other complexes crystallize in high-symmetry trigonal structures. In contrast, AF Mn_3Zn_2 crystallizes in the monoclinic $P2_1/n$ space group. As a consequence, the three Mn^{III} sites within the molecule are inequivalent, implying three different exchange coupling constants and three unique zfs tensors. It is this inequivalence that results in the relief of the spin frustration. Another consequence of the low-symmetry structure is that there are two differently oriented molecules within the unit cell, having their $[\text{Mn}_3^{\text{III}}-(\mu_3\text{-oxo})]$ planes misaligned by $\sim 32^\circ$. Consequently, there is a $\sim 32^\circ$ angle separating the local easy-axes of these two molecules, though the crystal obviously possesses a single easy-axis direction corresponding to the average for the two sites, i.e., $\sim 16^\circ$ from each of the local easy axes. This complicates the measurements and analysis. However, the crystals form as plates, with the average easy axis approximately perpendicular to the large, flat surfaces. Consequently, crystals were mounted for angle-dependent studies such that the rotation plane was perpendicular to the flat surfaces, thereby insuring that the field passes close to the average easy-axis. Finally, irrespective of the low symmetry, significant easy-axis anisotropy is anticipated on the basis of EPR studies of other members of this family, and because of the nearly parallel JT axes.

Sensitive low-field magnetization measurements were performed at dilution refrigerator temperatures on a small single-crystal by means of Hall-effect magnetometry [35]. The use of a vector magnet allowed for in-situ alignment of the applied field relative to the crystal. Magnetization hysteresis data were then collected at a sweep rate of 0.4 T/min in the temperature range from 30 mK to 1.3 K. High-field magnetic torque measurements were performed using a harmonic cantilever beam torquemeter with capacitive sensing; the sample was placed at the

edge of the cantilever beam. These measurements employed a 32 mm bore, 36 T resistive magnet at the National High Magnetic Field Laboratory (NHMFL) in Tallahassee, FL. Temperatures in the range from 0.3 to 10 K were achievable using a ^3He refrigerator. In order to ensure *in-situ* alignment of the magnetic field, the torque signal could be measured for different angles of application of the field relative to the crystal.

Multi-high-frequency EPR measurements were performed on a single crystal using a cavity perturbation technique spanning the frequency range from 50 to 600 GHz [36]. The temperature was regulated between 1.8 K and 20 K using helium gas flow cryostats. Two different magnet systems were employed for the EPR investigations: a 15 T vertical field superconducting solenoid for high field experiments; and a 7 T horizontal field superconducting split-pair for the highest frequency experiments due to its more compact size (hence a reduced optical path to the field center). *In-situ* sample rotation was also possible in both systems [37].

III(a) Low-Field Magnetization Studies

Figure 2 displays magnetization measurements performed in the range from 30 mK to 1.3 K, with the field applied perpendicular to the large flat surface of a single crystal, i.e., approximately parallel to the average easy-axis direction. Magnetic hysteresis is clearly observed at the lowest temperatures, with an onset at a blocking temperature, $T_B \approx 0.8$ K. This behavior implies molecular-level bistability due to a magnetic anisotropy barrier separating ‘spin-up’ and ‘down’ projection states [3]. Moreover, an obvious step in the hysteresis loops is seen at zero field (see derivatives in the inset to Fig. 2), which can be attributed to resonant quantum tunneling of the magnetization (QTM [38]). Meanwhile, the relaxation becomes temperature

independent below ~ 0.2 K (crossover temperature), which suggests that thermally activated processes are completely suppressed, and that the residual relaxation is due to direct processes involving the lowest-lying spin states, i.e., quantum tunneling and/or direct spin-lattice relaxation. It should be noted that these properties, which are normally associated with SMM behavior, have not been reported for the many other extensively studied AF Mn_3 complexes; indeed, similar investigations of a related high-symmetry AF Mn_3 complex (**4** in Ref. [17]) could detect no hysteresis to the lowest temperatures (35 mK) investigated. Finally, a fit of the high temperature magnetization to a Langevin function suggests a ground spin state $S = 1.7$ (≈ 2).

III(b) High-Frequency EPR Studies

As noted above, there are two differently oriented molecules in the unit cell of AF Mn_3Zn_2 , leading to two distinct high-field EPR signals with unique easy-axis directions [17]. Thus, angle-dependent EPR measurements were first performed so that the crystal could be aligned *in situ* (see [13] for details) for temperature and frequency-dependent measurements with the DC magnetic field applied approximately parallel to the average easy-axis direction, i.e., $\sim 16^\circ$ away from the local easy-axis (z-axis) of each molecule. As will be seen below, better sample alignment was achieved in the high-field magnet. Figs. 3 and 4 display temperature dependent measurements performed in the 7 and 15 T magnets, respectively, for several representative high frequencies (indicated in the figures). At the lower fields and frequencies, complicated patterns of relatively sharp peaks (dips in transmission) are observed at elevated temperatures. However, as the temperature is reduced to 2 K, most of this intensity vanishes, leaving behind only a few isolated peaks. Of these, three are relatively strong, which we label α , β , and γ . A weaker

resonance, labeled δ , is seen only at the lowest two frequencies. Only a single peak (α) is observed for all temperatures at frequencies of 500 GHz and above. On the basis of the temperature dependence, we associate the resonances labeled α , β , and γ with the ground state of the AF Mn_3Zn_2 molecule; δ is discussed further below. Meanwhile, the forest of peaks observed at elevated temperatures is easily understood as being due to transitions among the very many low-lying excited spin states expected for an AF molecule (see Figs 6 & 7 further below); similar high-temperature spectra were recorded (not shown) for many other frequencies below 244 GHz, down to the lowest frequency of 67 GHz employed in this study. We make no attempt in this work to account for the thermally excited EPR transitions, given (a) the inordinate number of peaks involved, and (b) the extreme sensitivity of the employed Hamiltonian to the positions of these peaks (*vide infra*). Nevertheless, their sharpness attests to the high quality of the crystal. From hereon, we focus on the labeled transitions α , β , γ ; and, to a lesser extent, δ .

The magnetic dipole selection rules, $\Delta S = 0$ and $\Delta m_s = \pm 1$, normally allow only a single ground state transition within a spin multiplet state. Consequently, the observation of three strong resonances as $T \rightarrow 0$ is somewhat unusual. However, recognizing that the $\text{Mn}^{\text{III}}\cdots\text{Mn}^{\text{III}}$ exchange is relatively weak in this complex ($|J| \sim |D|$), and that there remains appreciable spin frustration, it is clear that there should be significant state mixing between the densely spaced low-lying levels responsible for most of the EPR intensity (see Fig. 6 below), i.e., neither S nor m_s are likely to be good quantum numbers and, hence, the usual selection rules clearly break down [39]. In order to trace the origin of the ground state transitions, we performed detailed frequency dependent measurements at 2 K, spanning the interval from 67 to 600 GHz. Fig. 5 displays a 2D frequency versus field ‘map’ of the positions of resonances observed at each frequency. From such a plot, one can clearly identify the zero-field intercepts (i.e. the zfs)

associated with each of the labeled resonance branches. These may then be compared to simulations. However, before doing so, aspects of Figs. 3–5 require further explanation.

It is noticeable in Fig. 3(a) that, at 344 GHz, there appear to be two peaks labeled β , separated by about 0.8 T. Meanwhile, only a single β peak is observed at both frequencies in Fig. 4. The appearance of double peaks is a manifestation of the two molecular orientations, and the fact that the sample was not perfectly aligned for the high-frequency measurements performed in the split-pair magnet (Fig. 3). A similar behavior is found for the α resonance at higher fields, as seen in the inset to Fig. 3(b). These observations can be completely reproduced via simulations (not shown) that assume a $3^\circ - 5^\circ$ misalignment of the crystal. Since we are interested only in the zero-field intercepts of the various resonance branches, the data points in Fig. 5 represent the average positions in the cases of the double peaks, with error bars reflecting the associated uncertainty. Perfect alignment of the field along the average easy-axis direction is not easy. Nevertheless, the crystal used for the high-field studies was much better aligned. It is for this reason that many of the data points in the 4 – 7 T range in Fig. 5 have large error bars, whereas those at higher fields do not.

The solid lines in Fig. 5 are simple linear fits to the α , β , and δ resonance branches; the γ branch exhibits noticeable curvature and was, therefore, fit to a 2nd order polynomial. The sole purpose of these fits is to enable a determination of the associated zero-field intercepts (zfs): $\Delta_\alpha = 459(2)$ GHz; $\Delta_\beta = 196(2)$ GHz; $\Delta_\gamma = 66(2)$ GHz; $\Delta_\delta = 245(2)$ GHz. The average slope of the linear portions of the fits to the α , β , and γ resonances agree well with expectations for an axial system, with $\Delta m_S = +1$ and $g = 2.00$ (as expected for Mn^{III}), assuming a misalignment of $\sim 16^\circ$ of the easy axes due to the two molecular orientations. The curvature of the γ branch suggests repulsion between Zeeman levels, i.e., state mixing, as expected on the basis of the residual spin

frustration within the cluster. The slope of the linear fit to the δ resonance implies a g -value closer to 4.00 [3.60(7) when corrected for the sample alignment]. This suggests that it could either be a double quantum ($\Delta m_s = +2$) transition, or that it involves strongly admixed states. Moreover, it is apparent from Figs. 3(b) and 4(b) that the intensity of the δ resonance vanishes at higher fields as $T \rightarrow 0$, even though this is not the case at the lowest two fields/frequencies [Figs 3(a) and 4(a)]: note that it is completely absent at the expected location (see Fig. 5) in the 500 GHz data, and seen only at elevated temperatures at 419 GHz. Consequently, it is unlikely that the δ resonance involves an excitation from the ground state. We speculate instead that it involves an excitation from a low-lying state with $|m_s| < 2$ such that application of a field leads to further depopulation, and to a vanishing of the resonance at the lowest temperatures. For this reason, we do not consider Δ_δ directly in the following analysis. However, we do discuss its possible origin at the end of the article. Finally, one other excited state resonance, α' , is labeled in Fig. 4(b). This transition is related to α ($\Delta m_s = +1$, $m_s = -2$ to -1) through inversion of the applied field, i.e., it corresponds to a $\Delta m_s = -1$ transition from the metastable $m_s = +2$ state to the $m_s = +1$ state (from the point-of-view of a SMM, it corresponds to the ground state transition within the metastable potential well [3]). Consequently, it has the same zero-field intercept as α ; the same applies to β and β' (Fig. 5).

III(c) EPR Analysis

For the purposes of the ensuing analysis, we focus on the zero-field intercepts Δ_α , Δ_β and Δ_γ , which provide information on the separation between the ground state and the lowest lying excited states accessible via the magnetic dipole operator. As a starting point, we consider the

strong exchange limit in which the frustration is completely relieved by essentially setting one of the exchange interactions in the molecule to zero (equivalent to a linear AF trinuclear molecule), while the other two exchange constants remain large compared to the single-ion anisotropy. We have discussed exactly this situation theoretically in several recent articles [18,19,33]: the ground state may be treated as a rigid $S = 2$ spin, with a molecular anisotropy $D_{mol} = (69/49)d$, where d parameterizes the easy-axis (Ising-type) zfs associated with the individual Mn^{III} centers, assumed to be identical and parallel in this case. If we then assume that $d = -4.9$ K (this is the best fit value given below in section IV), we arrive at a value of $D_{mol} = -6.9$ K. We note that this value is nearly 6 times larger than the molecular D value found for the FM Mn_3^{III} molecules (≈ -1.2 K [17]). Consequently, AF Mn_3Zn_2 has the potential for a very significant magnetization reversal barrier ($= |DS^2|$), in spite of its low spin ($U_{\text{AF}} \approx 28$ K, compared to ~ 45 K for the FM examples).

The analysis outlined above involves many approximations, some of which are not well justified. Nevertheless, we shall see later that a more exact treatment tells essentially the same story. More importantly, the above approach provides a simple theoretical framework with which to make reasonable estimates for guiding experiments. Indeed, this proved particularly useful for the present investigations, suggesting a colossal ground state zfs, $\Delta_0 = (2S - 1)D_{mol} \approx 20.7$ K, or 430 GHz, for the $S = 2$ ground state. This is considerably larger than the values found for either $\text{Mn}_{12}\text{acetate}$ (~ 300 GHz [40]) or the Mn_3^{III} and Mn_6^{III} SMMs (both around 270 GHz [16-19,24,27,33]), necessitating the use of unusually high frequencies. This somewhat counterintuitive phenomenology can be attributed to the anisotropy dilution that occurs when spins are coupled together to produce high-spin (FM) molecules, i.e., D_{mol} decreases when S increases [19,29]. It is for this reason that AF Mn_3^{III} (with $S = 2$) can have a zfs ($\sim |2DS|$) which far exceeds that of the FM case (with $S = 6$), and a barrier for the molecular $S = 2$ state

approaching 60% of the theoretical maximum for three $S = 2$ spins. The total number of spins turns out to be more important for realizing good SMMs, which is why Mn_6^{III} is superior to FM Mn_3^{III} [19]. However, even then, the magnetization barrier scales approximately as S^1 , rather than S^2 , hence the barrier for Mn_6^{III} (with $S = 12$) is only twice that for FM Mn_3^{III} .

The strong exchange estimate of $\Delta_0 = 430$ GHz for the $S = 2$ state is rather close to the value determined experimentally for the α resonance branch in Fig. 5, i.e., $\Delta_\alpha = 459(2)$ GHz. We shall see below that this splitting does indeed belong to the nominal $S = 2$ ground state (nominal in the sense that S is not exact). This observation fills a major gap in earlier studies of an extensive family of related Mn_3 and Mn_6 complexes, where an effort was made to rationalize the differences in the anisotropies of FM and AFM molecules on the basis of a strong exchange (giant-spin) approximation [18,19,33]. This approach proved quite successful for the Mn_6 family due to the availability of high-quality EPR spectra for both the FM and AFM molecules [24]. However, a lack of good data for the AF molecules prevented such an analysis for the simpler Mn_3 complexes. At the time, this was correctly attributed to spin frustration in the AF Mn_3 triangles, which is mostly relieved in the AF Mn_6 molecules due to the reduced symmetry of the coupled $[\text{Mn}_3]_2$ triangles.

The small ($< 10\%$) difference between Δ_α and the strong exchange estimate for Δ_0 is of course due to the employed approximation, which also cannot account for the other two ground state resonance branches, β and γ . We therefore set out to simulate the spectrum using a multi-spin Hamiltonian that incorporates both the single-ion anisotropies and the exchange between the ions:

$$\hat{H} = \sum_i (d\hat{s}_{iz}^2 - g\mu_B\vec{B}\cdot\hat{s}_i) + \sum_{\substack{i,j \\ (i>j)}} J_{ij}\hat{s}_i\cdot\hat{s}_j. \quad (1)$$

Here, the lower-case \hat{s}_i correspond to single spin operators and \vec{B} denotes the applied field vector. The first summation parameterizes the magneto-anisotropy and Zeeman interactions associated with the individual Mn^{III} centers. We consider purely easy-axis (Ising-type) single-ion anisotropy and assume this to be the same for all three Mn^{III} ions, and parallel to z . The model is further simplified by assuming an isotropic Zeeman interaction ($g = 2.00$) for all three ions. Finally, the 2nd summation parameterizes the isotropic coupling between the three spins, allowing the possibility of three different values of the exchange constants, J_{ij} . In spite of several simplifying assumptions, the Hamiltonian of Eq. (1) contains the two key ingredients relevant to the present study: (i) it is possible to relieve the spin frustration via appropriate choices of the three exchange constants; and (ii) there is no restriction on the relative magnitudes of d and J_{ij} .

Previously reported magnetic measurements provide strong evidence that this compound possesses a reasonably isolated $S \approx 2$, $m_S \approx \pm 2$ ground state (see comparison between low and high-symmetry complexes **3** and **4** in Figs. 6 and 7 in Ref. [17]). Indeed, the magnetic measurements and structural data were the motivating factors behind the present investigation. Moreover, from the outset (see above), our expectation was that the ground state transition associated with this $S \approx 2$ state (i.e., $m_S = \pm 2$ to ± 1) should have a zfs, $\Delta > 400$ GHz. For these reasons, we approached the task of simulating the data by assuming that the α resonance branch corresponds to this transition. Nevertheless, there is another compelling piece of evidence in support of this assignment. Fig. 4(b) reveals that the intensity of the excited state α' resonance overtakes those of the ground state β and γ resonances very quickly. This suggests that the matrix

element for the α' resonance, which should be the same as that for the α resonance, is significantly stronger than the matrix elements for β and γ [41]. Therefore, our efforts to simulate the EPR data focused first and foremost on the α resonance branch. We shall see below that, in doing so, we could make robust, testable predictions concerning the proximity of excited spin states relative to the nominal $S = 2$ ground state.

On the basis of EPR studies of related FM complexes, which suggest that d is relatively insensitive to the structural distortions that affect the exchange constants [19], we restricted the axial parameter to values in the range from 4-6 K during searches for the best simulation (see below [42]). Thus, optimization of the simulations was achieved primarily through variation of the three exchange coupling constants, J_{ij} ; again, searches were limited to J values below 25 K on the basis of published susceptibility data [17] (see also below). Figure 6 displays the best simulation (*vide infra*) of the zero-field eigenvalue spectrum. Figure 6(b) shows an expanded view of the lowest energy states responsible for most of the low temperature EPR intensity; the colors and sizes of the data points have been coded according to the expectation value of $\sqrt{S(S+1)}$. Since only axial anisotropy (d , with parallel orientations on the three Mn^{III} sites) was employed for the simulations, m_s remains an exact quantum number whereas S clearly is not. The presumed α , β and γ resonances have been marked on the figure. The corresponding zfs values between the ground and relevant excited states are: $\Delta_\alpha = 459$ GHz, $\Delta_\beta = 196$ GHz and $\Delta_\gamma = 69$ GHz. These compare remarkably well with the experimental values given in Section III(b); horizontal solid black lines have been included in Fig. 6 to mark the experimentally determined excitation energies from the ground state. As can be seen, the α resonance involves states with similar expectation values for the total spin, i.e., the states belong to a nominal $S = 2$

ground state, as indicated by the dashed curve. The β and γ resonances connect states with rather different total spin values. Nevertheless, the matrix elements for these transitions are non-negligible (*vide infra*). We discuss these simulations in more detail in section IV.

III(d) High-Field Magnetic Torque Measurements

While performing simulations of the EPR data, we noticed that it should be possible to induce a spin-crossover transition from a low-spin state (nominally $S = 2$) to a maximal spin state ($S = 6$) at magnetic fields achievable at the NHMFL. This is illustrated by means of Fig. 7, which displays the magnetic field dependence of the low-energy portion of the spectrum in Fig. 6; the simulations take into account the two molecular orientations by assuming that the field is tilted 16° away from the easy axes of each molecule. The ground state undergoes a succession of transitions between about 28 T and 35 T (denoted by vertical black arrows), seen more clearly in the inset, which displays the calculated magnetic moment per molecule (in units of $g\mu_B$) for several low temperatures. Realizing that high-field measurements would provide an additional constraint on the spin Hamiltonian parameters [Eq. (1)], we conducted high-field magnetic torque measurements on a single crystal of AF Mn_3Zn_2 . Provided that the torque signal is not too large, one may assume a linear response in which the measured capacitance of the torquemeter is proportional to the deflection of the cantilever beam which, in turn, is proportional to the torque ($\tau = |\vec{M} \times \vec{B}|$) on the sample. The crystal was first oriented *in situ* so that the applied field was aligned close to the direction of minimum torque signal [43]. Based on the initial placement of the flat crystal on the cantilever, it was assumed that this field orientation was close to the average easy-axis direction. Figure 8 shows a plot of the capacitance of the cantilever

magnetometer versus magnetic field strength, for temperatures varying from 300 mK to 10 K, and with the field swept at a constant rate of 3 T/min.

Magnetic torque measurements are complicated by the fact that one should have *a priori* knowledge of the full magnetic anisotropy tensor in order to interpret the results, i.e., unlike magnetization or susceptibility, torque is not a true thermodynamic quantity. Even a knowledge of the optimum parameters of Eq. (1) is insufficient, because the torque signal in the vicinity of the level crossings (spin crossover transitions) is highly sensitive to any level mixing and, hence, to the transverse anisotropy terms (which we ignore in our simulations due to an insufficient number of experimental constraints) [44]. Nevertheless, one expects the low-temperature torque signal to display a monotonic dependence on the magnetic field strength in situations where the spin ground state remains well isolated from excited spin states. Consequently, the strong low-temperature oscillations observed between ~ 28 and 35 T in Fig. 8 are a sure signature of multiple spin crossover transitions. The oscillations reside on a fairly monotonous background of steadily increasing torque, signifying the gradual population of excited spin states, all the way up to $S = 6$ (note that a similar trend is observed with increasing temperatures at fields below 20 T). The oscillations, meanwhile, reflect the competition between diagonal and off-diagonal components of the anisotropy tensor. In fact, it is noticeable that the oscillation just below 30 T is strongest at slightly elevated temperatures (0.9 K), suggesting that it might be due to a crossing between spin states located just above the ground state.

IV. Discussion

While it is not possible to make precise assignments of the transitions associated with the torque oscillations seen in Fig. 8, the results provide compelling support for the Hamiltonian parameters estimated initially on the basis of the EPR data, i.e., the simulation in Fig. 6 accounts well for the zero-field intercepts associated with the α , β and γ resonances, *and* the field range where the torque oscillations are observed. We emphasize that the locations of the spin-crossover transitions were used as an additional discriminator when determining the best fit/simulation: a four-dimensional $\chi^2(d, J_1, J_2, J_3)$ surface was first computed through comparisons of the Δ_α , Δ_β and Δ_γ values with the simulations; this surface was then searched to find minima which were then discarded if they did not produce spin-crossover transitions in the appropriate magnetic field interval (from 25 to 36 T). As noted above, the search routine was restricted to a parameter space bounded by values that were informed by several other considerations, e.g., susceptibility measurements [17], and anisotropy values determined for similar compounds [19,42,45]. In addition, the magnetic dipole matrix elements were computed for all transitions from the ground state (lowest energy state) and used as an additional discriminator [46], thereby eliminating many unphysical parameter sets. Thus, in effect, the results displayed in Fig. 6 represent a ‘best fit’ to a broad range of measurements.

The ‘best fit’ was achieved with the following parameters: $d = -4.9$ K, $J_1 = 6.9$ K, $J_2 = 7.3$ K and $J_3 = 11.8$ K. Indeed, no other parameter sets were found to give a satisfactory account of the combined measurements within the constraints described above. It is not possible to assign the obtained J values to the individual Mn...Mn contacts within the molecule. Therefore, we make no attempt to rationalize the differences on the basis of the structure, though we hope that the present investigation might motivate future computational studies targeted at this issue.

Meanwhile, the obtained d value is close to those found for the related FM Mn_3Zn_2 complexes and other similar compounds ([17-20,45]), lending further weight to this parameterization.

The obtained exchange constants are not entirely incompatible with those deduced from fits to magnetic susceptibility data ($J_1 \sim 0$, $J_2 = J_3 = 10$ K [17]). Nevertheless, as a consistency check, we simulated the temperature-dependent susceptibility for a powder sample using the ‘best fit’ zfs parameters. We found that near perfect agreement could be achieved by reducing the g -factor to 1.93 (inset to Fig. 8), corresponding to a $\sim 3\%$ reduction over the expected value of ~ 2.00 (or slightly lower). We note that it is extremely common to find published fits to magnetic data that under-report g -values (by as much as 10%). This is likely due to quantitative errors associated with estimations of absolute susceptibility that are sensitive to errors in precise sample weight and solvent content after drying. The most important thing is that the simulation sits exactly on the data when scaled vertically by the reduced g -value, because this indicates that our parameterization correctly captures the temperature dependence of the susceptibility, even if the absolute value is off by a few percent. It should be emphasized that fits to susceptibility data are notoriously unreliable in cases such as this one where there is not a clear separation of the energy scales associated with the exchange and anisotropy within the cluster. Such fits simply involve way too many parameters and the susceptibility data contains too little information [19]. Therefore, it is no surprise to us that the current EPR parameterization does not agree with the earlier fits to susceptibility data.

As anticipated on the basis of the broken C_3 symmetry of the triangle, there is a significant difference between the three exchange coupling constants: J_1 and J_2 are ~ 7 K, while J_3 is almost double (~ 12 K). This difference, along with the relative magnitudes of d and the three J s, has a significant effect in terms of localizing the spin moments on the individual Mn^{III} sites in the

molecule. This can be examined by computing the expectation values, $\langle m_i \rangle$ and $\langle m_i^2 \rangle^{1/2}$, at the three sites ($i = 1$ to 3). In particular, in the case of the lowest lying molecular $m_S = \pm 2$ doublet, the departure of $\langle m_i^2 \rangle^{1/2}$ from 2.00 provides a measure of the spin delocalization. For the obtained parameter set, $\langle m_1^2 \rangle^{1/2} = 1.87$, $\langle m_2^2 \rangle^{1/2} = 1.98$ and $\langle m_3^2 \rangle^{1/2} = 1.85$, where the stronger exchange constant, J_3 , couples spin 3 to spin 1. These numbers indicate some delocalization (weak entanglement) between the stronger coupled spins 1 and 3, while spin 2 is almost completely localized along z . Increasing J_3 increases the entanglement between spins 1 and 3 without affecting spin 2 significantly ($\langle m_1^2 \rangle^{1/2} = \langle m_3^2 \rangle^{1/2} = 1.62$ for $J_3 = 30$ K). On the other hand, reducing J_3 actually increases the localization on sites 1 and 3: for $J_1 = J_2 = J_3 = 6$ K, $\langle m_i^2 \rangle^{1/2} = 1.95$ ($i = 1, 2$ and 3). The reason is because the Ising-like anisotropy ($d < 0$) really dominates over the Heisenberg interaction as the J s are weakened.

Based on the above considerations, one can conclude that there are two important factors that contribute to the unique low-temperature properties of this Mn_3 complex: (i) the appreciable easy-axis (Ising) anisotropy ($d \sim J_i$) and parallel disposition of the Mn^{III} JT axes results in an approximately collinear arrangement of the spins in the ground state; and (ii) the unequal J s relieve the spin frustration, thus reducing the density of low-lying levels so that the ground state is reasonably well isolated. We argue that it is these factors that are necessary in order to observe magnetization hysteresis and the high quality EPR spectra.

We return briefly to the giant spin description of the ground state. The expectation value, $\langle \sqrt{S(S+1)} \rangle \approx 2.5$, for the states connected by the α resonance, suggesting a total spin value not far from 2.0. The black curve in Fig. 6(b) is a 4th order polynomial fit to the five m_S states associated with the ground spin multiplet. The obtained 2nd and 4th order coefficients are -11.3 K

and +0.785 K. These numbers can be equated with the parameters D and B in the fourth order effective spin Hamiltonian, $\hat{H} = D\hat{S}_z^2 + B\hat{S}_z^4$. However, one should be careful making direct comparisons with the usual Stevens operator formalism due to the very significant fourth order contribution to the spectrum; indeed, the magnitude of the D value estimated in this way is 64% larger than predicted on the basis of the strong exchange approximation in Section III(c). However, further inspection of Fig. 6(b) reveals that the $m_s = 0$ sub-level associated with the ground state multiplet is rather more strongly mixed in comparison to the $m_s \neq 0$ sub-levels. Indeed, it is this spin state mixing that gives rise to the 4th order contribution to the effective spin Hamiltonian [19,47]. If one instead discards the $m_s = 0$ sub-level and fits a 2nd order polynomial to the remaining $m_s \neq 0$ sub-levels, a D parameter of -7.35 K is obtained, which is only 6.5% larger than the value estimated in Section III(c) on the basis of the strong exchange approximation. The main purpose of these comparisons is to demonstrate that the ground state of the AF Mn_3Zn_2 molecule can reasonably be described in terms of a strong exchange, or giant spin approximation, with $S = 2$, and that Δ_α corresponds to the zfs within this ground state.

All that remains is to examine the remaining low temperature ‘inter-spin multiplet’ transitions β and γ . On the basis of the optimum parameterization deduced above, the matrix elements associated with these resonances are significantly weaker than the α resonance (by a factor of 4 for β and by two orders of magnitude for γ). However, we find that these matrix elements are highly sensitive to small variations of the exchange parameters. Moreover, addition of relatively weak 2nd order transverse anisotropy, $e\left(\hat{S}_x^2 - \hat{S}_y^2\right)$, at the Mn^{III} sites makes a huge difference to these matrix elements as well; we note that such anisotropy certainly exists, but that there is insufficient data for it to be included in any realistic analysis. While this situation is far

from satisfactory, we have made several searches by hand around the parameter values given above, with the addition of a single transverse anisotropy parameter, e , and we do find that it is possible to generate matrix elements that mimic the experiments, i.e., comparable intensities for β and γ , and a considerably stronger intensity for α .

By the same token, one finds several higher lying $m_s = \pm 1$ states that are connected to the ground state by non-negligible matrix elements (within a factor of 5-10 of α). However, these are not observed in the EPR experiments. The first of these transitions occur in the ~ 550 GHz range. As can be seen in the inset to Fig. 3, it is possible that the signal-to-noise ratio is insufficient to pick out such weak resonances at the highest frequencies, where the spectrometer is approaching the limits of its operating range for crystals of this size. It is also possible that the calculated matrix elements are artificially high for the reasons discussed above; note that inclusion of 2nd order transverse anisotropy can both increase and decrease the matrix elements. Clearly, future enhancements in the spectrometer would enable further examination of this point.

Finally, we come back to the δ resonance that we believe originates from a low-lying excited state with $|m_s| < 2$. Such a transition does in fact exist within the obtained parameterization, as indicated by the gray arrow in Fig. 6. The dashed horizontal line, labeled δ , denotes the experimentally determined excitation energy (Δ_δ) from the lowest lying $m_s = -1$ state. The agreement is relatively good, and the involved states have similar S character (similar size/color). Moreover, the lowest lying $m_s = \pm 1$ states reside just 3 K above the ground state at zero field. Therefore, they should be reasonably well populated at zero field, even at the lowest temperatures employed in this study. However, upon application of a 4 T field ($//z$), the

separation from the ground state increases to ~ 9 K, again consistent with the observation of the δ resonance at 4 T in Fig. 4(b) only when the temperatures approaches 9 K.

V. Summary and Conclusions

We present extensive high-frequency EPR and low-temperature magnetic measurements, at both low and high magnetic fields, on crystals of an AF Mn_3 molecular nanomagnet. We demonstrate that the reduced symmetry of this molecule relieves the spin frustration inherent to most other AF μ_3 -oxo-centered triangular Mn_3^{III} complexes, resulting in a relatively isolated $S = 2$ ground state that experiences a very significant axial anisotropy due to the near collinearity of the JT axes on the three Mn^{III} ions. These properties give rise to magnetization hysteresis below a blocking temperature of 0.8 K, and extremely clean EPR spectra. The hysteresis is indicative of SMM behavior, while extensive multi-frequency EPR measurements have enabled important comparisons between related FM and AF Mn_3 systems that had previously been lacking [19].

Simulations of the EPR data employing a multi-spin Hamiltonian motivated a search for spin-crossover transitions at high magnetic fields. To this end, magnetic torque measurements have been performed in fields of up to 35 T, revealing the predicted crossover transitions in the expected field range. The combined magnetic and EPR data sets have allowed for careful simulation of the spectrum of AF Mn_3Zn_2 .

VI. Acknowledgements

The authors acknowledge support from the NSF, specifically E.d.B. from DMR-0747587 and

S.H from DMR-0804408. Work performed at the NHMFL is supported by the State of Florida and the NSF through award DMR-0654118.

VII. References Cited

* shill@magnet.fsu.edu

- ¹ R. Sessoli, D. Gatteschi, A. Caneschi and M. A. Novak, *Nature* **365**, 141 (1993).
- ² R. Sessoli, H. L. Tsai, A. R. Schake, S. Wang, J. B. Vincent, K. Folting, D. Gatteschi, G. Christou and D. N. Hendrickson, *J. Am. Chem. Soc.* **115**, 1804 (1993).
- ³ D. Gatteschi, R. Sessoli and J. Villain, *Molecular Nanomagnets* (Oxford University Press, Oxford, 2006).
- ⁴ *Single-Molecule Magnets and Related Phenomena*, Structure and Bonding Vol. **122**, Ed. R. E. P. Winpenny (Springer, Heidelberg, 2006).
- ⁵ *Magnetism in Condensed Matter*, Stephen Blundell, Oxford University Press (Oxford, 2001).
- ⁶ J. B. Vincent, H. R. Chang, K. Folting, J. C. Huffman, G. Christou, D. N. Hendrickson, *J. Am. Chem. Soc.* **109**, 5703 (1987).
- ⁷ J. K. McCusker, H. G. Jang, S. Wang, G. Christou, D. N. Hendrickson, *Inorg. Chem.* **31**, 1874 (1992).
- ⁸ S. G. Sreerama and S. Pal, *Inorg. Chem.* **41**, 4843 (2002).
- ⁹ L. F. Jones, G. Rajaraman, J. Brockman, M. Murugesu, J. Raftery, S. J. Teat, W. Wernsdorfer, G. Christou, E. K. Brechin, D. Collison, *Chem. Eur. J.* **10**, 5180 (2004).
- ¹⁰ T. C. Stamatatos, D. Foguet-Albiol, C. C. Stoumpos, C. P. Raptopoulou, A. Terzis, W. Wernsdorfer, S. P. Perlepes, and G. Christou, *J. Am. Chem. Soc.* **127**, 15380-15381 (2005).
- ¹¹ C. J. Milios, A. G. Whittaker and E. K. Brechin, *Polyhedron*, **26**, 1927 (2007).
- ¹² C. J. Milios, P. Wood, S. Parsons, D. Foguet-Albiol, C. Lampropoulos, G. Christou, S. P. Perlepes, E. K. Brechin, *Inorg. Chim. Acta* **360**, 3932 (2007).
- ¹³ T. C. Stamatatos, D. Foguet-Albiol, S.-C. Lee, C. C. Stoumpos, C. P. Raptopoulou, A. Terzis, W. Wernsdorfer, S. O. Hill, S. P. Perlepes, and G. Christou., *J. Am. Chem. Soc.* **129**, 9484-9499 (2007).
- ¹⁴ H.-B. Xu, B.-W. Wang, F. Pan, Z.-M. Wang, S. Gao, *Angew. Chem., Int. Ed.* **46**, 7388

- (2007).
- ¹⁵ C.-I. Yang, W. Wernsdorfer, K.-H. Cheng, M. Nakano, G.-H. Lee and H.-L. Tsai, *Inorg. Chem.* **47**, 10184-10186 (2008).
 - ¹⁶ P. L. Feng, C. Koo, J. J. Henderson, M. Nakano, S. Hill, E. del Barco and D. N. Hendrickson, *Inorg. Chem.* **47**, 8610-8612 (2008).
 - ¹⁷ P. L. Feng, C. Koo, J. Henderson, P. Manning, M. Nakano, E. del Barco, S. Hill and D. N. Hendrickson, *Inorg. Chem.* **48**, 3480-3492 (2009).
 - ¹⁸ R. Inglis, S. M. Taylor, L. F. Jones, G. S. Papaefstathiou, S. P. Perlepes, S. Datta, S. Hill, W. Wernsdorfer and E. K. Brechin, *Dalton Trans.* **2009**, 9157-9168 (2009).
 - ¹⁹ S. Hill, S. Datta, J. Liu, R. Inglis, C. J. Milios, P. L. Feng, J. J. Henderson, E. del Barco, E. K. Brechin, D. N. Hendrickson, *Dalton Trans.* **39**, 4693-4707 (2010).
 - ²⁰ J. J. Henderson, C. Koo, P. L. Feng, E. del Barco, S. Hill, I. S. Tupitsyn, P. C. E. Stamp, D. N. Hendrickson, *Phys. Rev. Lett.* **103**, 017202 (2009).
 - ²¹ J. Liu, E. del Barco, S. Hill, in preparation.
 - ²² C. J. Milios, A. Vinslava, P. A. Wood, S. Parsons, W. Wernsdorfer, G. Christou, S. P. Perlepes, E. K. Brechin, *J. Am. Chem. Soc.* **129**, 8-9 (2007).
 - ²³ C. J. Milios, A. Vinslava, W. Wernsdorfer, S. Moggach, S. Parsons, S. P. Perlepes, G. Christou and E. K. Brechin, *J. Am. Chem. Soc.* **129**, 2754 (2007).
 - ²⁴ R. Inglis, L. F. Jones, C. J. Milios, S. Datta, A. Collins, S. Parsons, W. Wernsdorfer, S. Hill, S. P. Perlepes, S. Piligkos and E. K. Brechin, *Dalton Trans.* **2009**, 3403-3412 (2009).
 - ²⁵ S. Carretta, T. Guidi, P. Santini, G. Amoretti, O. Pieper, B. Lake, J. van Slageren, F. El Hallak, W. Wernsdorfer, H. Mutka, M. Russina, C. J. Milios, E. K. Brechin, *Phys. Rev. Lett.* **100**, 157203 (2008).
 - ²⁶ S. Bahr, C. J. Milios, L. F. Jones, E. K. Brechin, V. Mosser, and W. Wernsdorfer, *Phys. Rev. B* **78**, 132401 (2008).
 - ²⁷ O. Pieper, T. Guidi, S. Carretta, J. van Slageren, F. El Hallak, B. Lake, P. Santini, G. Amoretti, H. Mutka, M. Koza, M. Russina, A. Schnegg, C. J. Milios, E. K. Brechin, A. Julià and J. Tejada, *Phys. Rev. B* **81**, 174420 (2010).
 - ²⁸ J. Cano, T. Cauchy, E. Ruiz, C. J. Milios, C. C. Stoumpos, T. C. Stamatatos, S. P. Perlepes, G. Christou and E. K. Brechin, *Dalton Trans.* **2008**, 234-240 (2008).
 - ²⁹ O. Waldmann, *Inorg. Chem.* **46**, 10035-10037 (2007).

- ³⁰ E. Ruiz, J. Cirera, J. Cano, S. Alvarez, C. Loose, and J. Kortus, *Chem. Commun.* **2008**, 52 (2008).
- ³¹ This is attributable to extremely high quality crystals that contain no disordered solvate molecules; see also J. Lawrence, E.-C. Yang, R. Edwards, M. M. Olmstead, C. Ramsey, N. S. Dalal, P. K. Gantzel, S. Hill, D. N. Hendrickson, *Inorg. Chem.* **47**, 1965-1974 (2008).
- ³² Prior to the present investigation, we made attempts at studying a considerable number of AF Mn_3^{III} molecules from three different sources. In nearly all cases, only broad featureless peaks were observed at or around the $g = 2$ position (see e.g. Ref. [17]). In one other recent AF example, relatively low frequency (52 GHz) EPR spectra are presented that display a series of broad widely spaced peaks signifying appreciable zfs [18].
- ³³ S. Datta, E. Bolin, R. Inglis, C. J. Milios, E. K. Brechin and S. Hill, *Polyhedron* **28**, 1911-1916 (2009).
- ³⁴ J. Schnack, *Dalton Trans.* **39**, 4677-4686 (2010).
- ³⁵ A. D. Kent, S. von Molnar, S. Gider, and D. D. Awschalom, *J. Appl. Phys.* **76**, 6656 (1994).
- ³⁶ M. Mola, S. Hill, P. Goy and M. Gross, *Rev. Sci. Inst.* **71**, 186 (2000).
- ³⁷ S. Takahashi and S. Hill, *Rev. Sci. Inst.* **76**, 023114 (2005).
- ³⁸ E. M. Chudnovsky and J. Tejada, *Macroscopic Tunneling of the Magnetic Moment* (Cambridge University Press, Cambridge, 2005).
- ³⁹ S. Datta, O. Waldmann, A. D. Kent, V. A. Milway, L. K. Thompson, S. Hill, *Phys. Rev. B* **76**, 052407 (2007).
- ⁴⁰ G. Redler, C. Lampropoulos, S. Datta, C. Koo, T. C. Stamatatos, N. E. Chakov, G. Christou and S. Hill, *Phys. Rev. B* **80**, 094408 (2009); and references therein.
- ⁴¹ We note that it was not possible to compare α , β and γ directly in a single measurement. One has to be careful comparing intensities from one frequency to another, because the absolute sensitivity of the spectrometer is not calibrated. Therefore, one can only reliably compare intensities recorded at a single frequency. Nevertheless, the signal-to-noise ratio of the spectrometer diminishes with increasing frequency. Consequently, the fact that a very strong α resonance is observed at 500 GHz suggests that it is a strong transition.
- ⁴² References [16,17,20] suggest d values in the range from 4.2 to 4.6 K for the FM complexes, i.e., within the bounds explored for the simulations. We note also that d values above 5 K are

unprecedented for octahedrally coordinated Mn(III); see J. Krzystek, A. Ozarowski and J. Telsler, *Coord. Chem. Rev.* **250**, 2308-2324 (2006).

- ⁴³ This was achieved by first recording the angle-dependent torque signal at a low magnetic field (1 T), then returning close to the orientation (within 1°) of minimum torque signal. While this leads to a negligible torque at low fields (since \vec{M} approximately parallel to \vec{B}), a small misalignment is unavoidable, resulting in strong torque at high fields.
- ⁴⁴ O. Waldmann, S. Carretta, P. Santini, R. Koch, A. G. M. Jansen, G. Amoretti, R. Caciuffo, L. Zhao and L. K. Thompson, *Phys. Rev. Lett.* **92**, 096403 (2004).
- ⁴⁵ H. M. Quddusi, J. Liu, S. Singh, K. J. Heroux, E. del Barco, S. Hill, and D. N. Hendrickson, *Phys. Rev. Lett.* (in press).
- ⁴⁶ A cut-off of $\langle m | \hat{S}_x | m' \rangle^2 > 0.03$ was employed; for reference, the matrix element for the α resonance is ~ 2.5 .
- ⁴⁷ A. Wilson, J. Lawrence, E-C. Yang, M. Nakano, D. N. Hendrickson and S. Hill, *Phys. Rev. B* **74**, R140403 (2006).

FIGURE CAPTIONS

Fig. 1. (color online) Structure of the AF Mn_3Zn_2 molecule viewed from slightly above the plane of the triangular Mn_3 core (a) and from directly above this plane (b). The atoms have been labeled in the figure, and are also color coded as follows: Mn – magenta; Zn – dark red; O – red; N – light blue; and C – grey. Hydrogen atoms are omitted for clarity.

Fig. 2. (color online) Magnetization (M) hysteresis as a function of the applied magnetic field at different temperatures below the blocking temperature; M_S represents the low-field (< 10 T) saturation magnetization. The inset shows the field derivative of the magnetization curves.

Fig. 3. (color online) Temperature dependent high-frequency EPR spectra obtained in the 7 T horizontal-field, split-pair magnet. In the main panels, the frequencies are indicated, and data were recorded at the same five temperatures with the upper traces corresponding to 10 K; the ground state resonances observed at the lowest temperatures have been labeled accordingly. The inset to (b) shows the highest frequency (593 GHz) data obtained in this study, revealing the α resonance at a temperature of 2.0 K.

Fig. 4. (color online) Temperature dependent high-frequency EPR spectra obtained in the 17 T vertical-field magnet. The frequencies in (a) and (b) are indicated, and data were recorded at the same five temperatures, with the upper traces corresponding to 10 K. Several of the main resonances have been labeled (see main text).

Fig. 5. (color online) 2D frequency versus field ‘map’ of the positions of resonances observed at many frequencies in the range from 60 to ~ 600 GHz with the field applied parallel to the average

easy axis direction; the horizontal dashed (red) and dot-dashed (blue) lines indicate the measurements displayed in Figs. 3 and 4, respectively. The data points have been color and shape coded according to the associated resonance branches – see legend. The solid lines are linear (α , β , δ) and 2nd order polynomial (γ) fits to the corresponding data points, from which accurate determinations of the zfs may be deduced.

Fig. 6. (color online) (a) Best simulation of the zero-field eigenvalue spectrum generated from Eq. (1). The states are plotted versus their associated m_S quantum number. The highest energy states belong to well defined spin multiplets, a few of which have been labeled accordingly. The red box highlights the low-energy region of the spectrum that has been expanded in (b). The colors and sizes of the data points in (b) have been coded according to the expectation value of $\sqrt{S(S+1)}$, with radii proportional to this value (see legend also). The solid black curve is a 4th order polynomial fit to the states that belong to the lowest-lying $S = 2$ ground state multiplet (see main text for further explanation of this fit). The presumed α (red arrow), β and γ (blue arrows) resonances have been marked on the figure; we also make a tentative assignment for the δ resonance (grey arrow). The solid horizontal black lines correspond to the experimentally determined excitation energies (Δ_α , Δ_β and Δ_γ) above the ground state; the dashed horizontal line corresponds to the energy separation Δ_δ from the lowest lying $m_S = -1$ state.

Fig. 7. (color online) Simulated Zeeman diagram representing the field dependence of the low energy portion of the spectrum displayed in Fig. 6; the simulations take into account the two molecular orientations by assuming that the field is tilted 16° away from the easy axes of each molecule. The red vertical arrow labeled α indicates the excitation from the nominal $S = 2$,

$m_S = 2$ ground state (thick red line labeled $|2,2\rangle$), to the $m_S = 1$ excited state (thin red line) within this same multiplet. The blue vertical arrows labeled β and γ indicate excitations from the ground state to excited spin multiplets (thin blue lines). The vertical black arrows above 25 T denote the locations of spin crossover transitions from the $|2,2\rangle$ state at low field, to the presumed $|6,6\rangle$ state (thick black line) at high fields. The inset displays the simulated high-field magnetization.

Fig. 8. (color online) Capacitance of the cantilever torquemeter as a function of temperature and magnetic field. The field sweep rate is 3 T/min. The change in capacitance is proportional to the magnetic torque on the sample. The lower inset displays temperature dependent susceptibility data for a powder sample (from [17]), together with a simulation obtained using the zfs parameters inferred from the EPR analysis (see main text for further explanation).

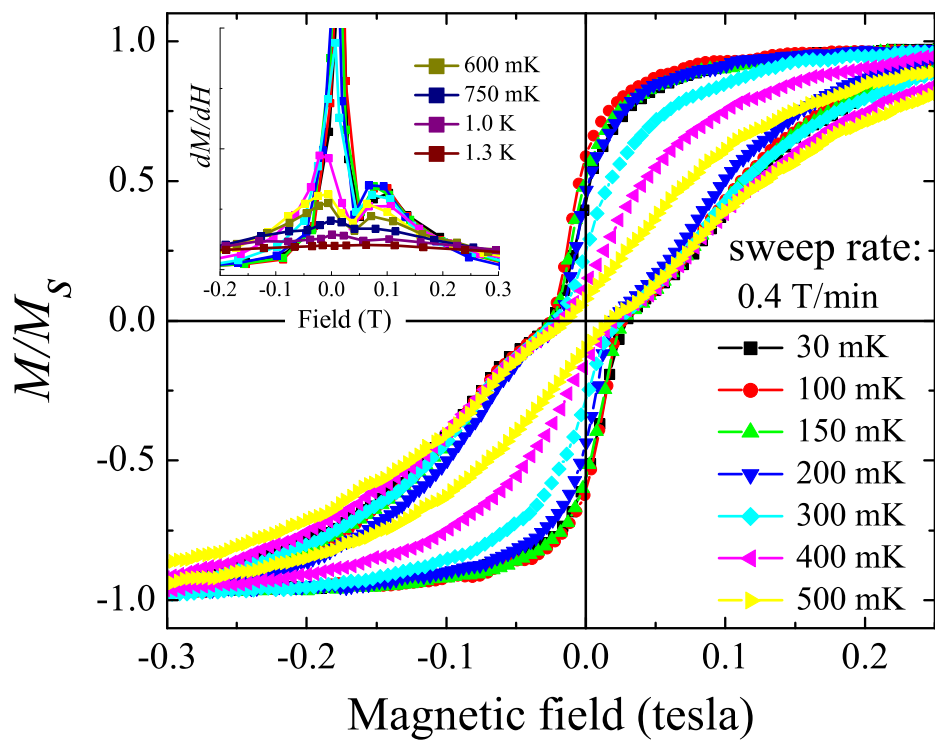


Fig. 2, Liu et al.

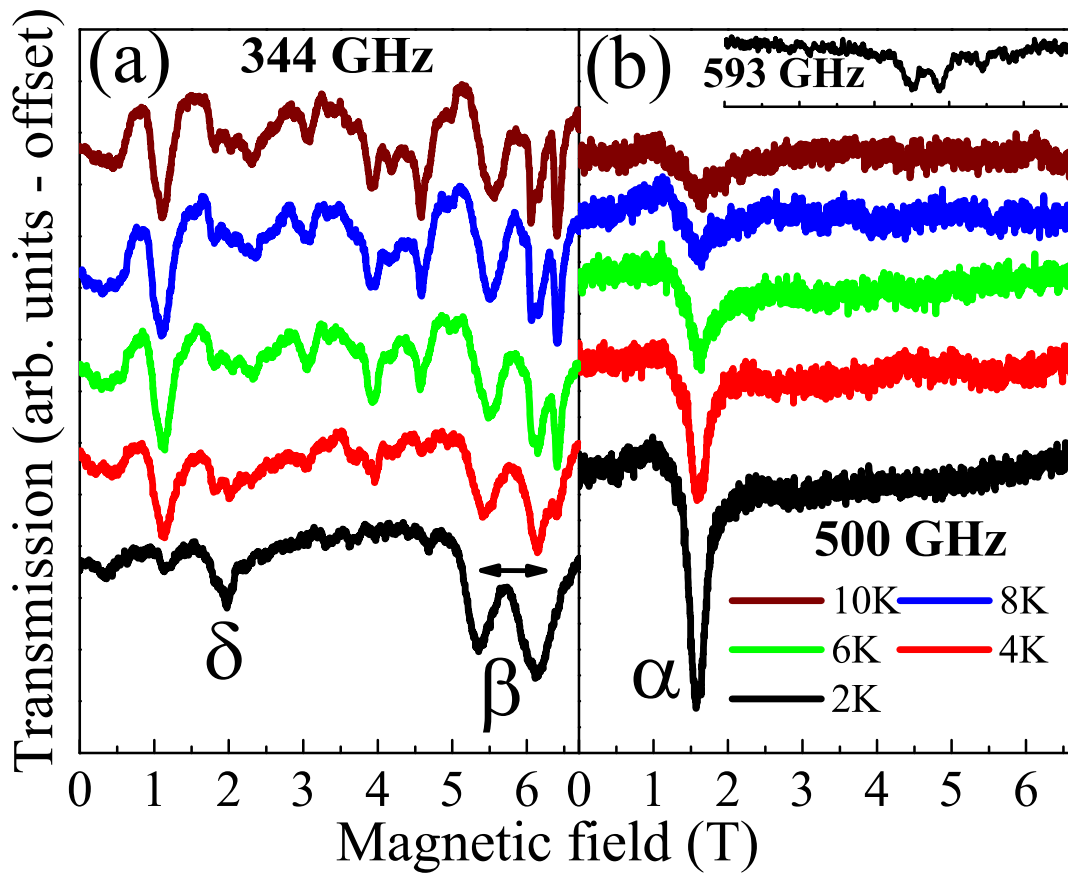


Fig. 3, Liu et al.

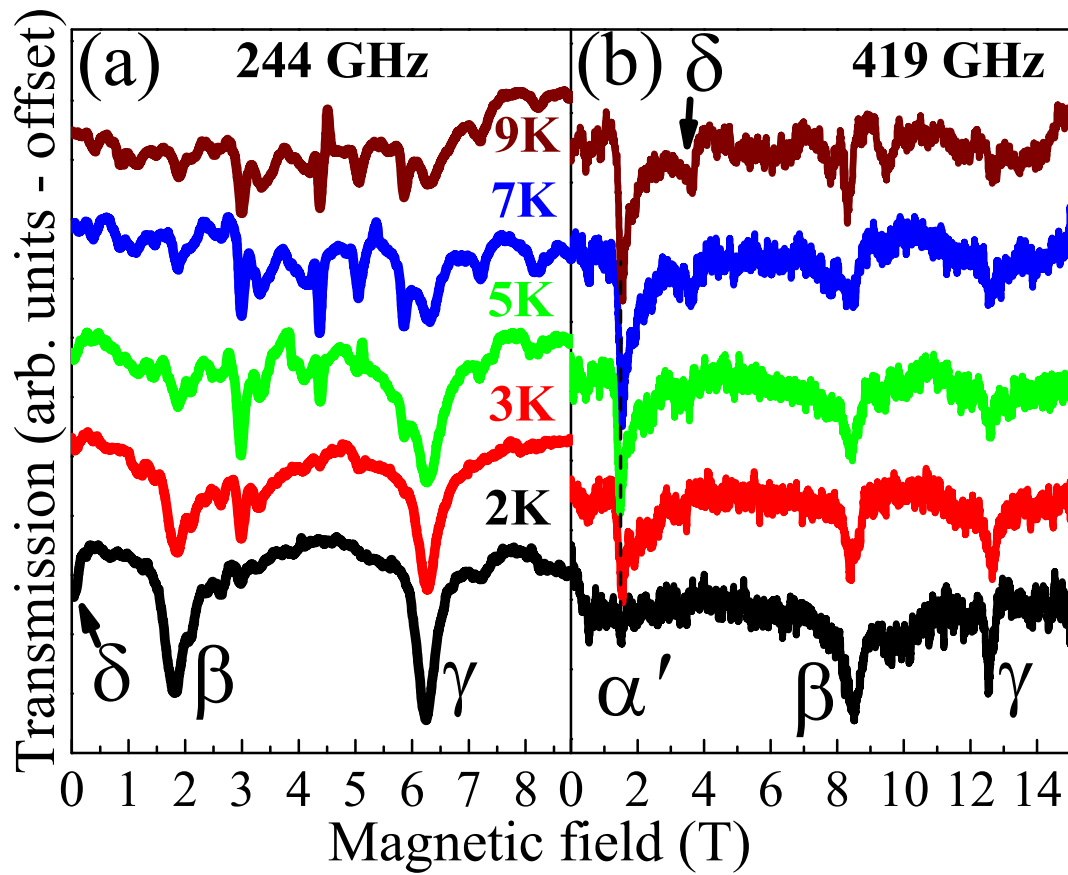


Fig. 4, Liu et al.

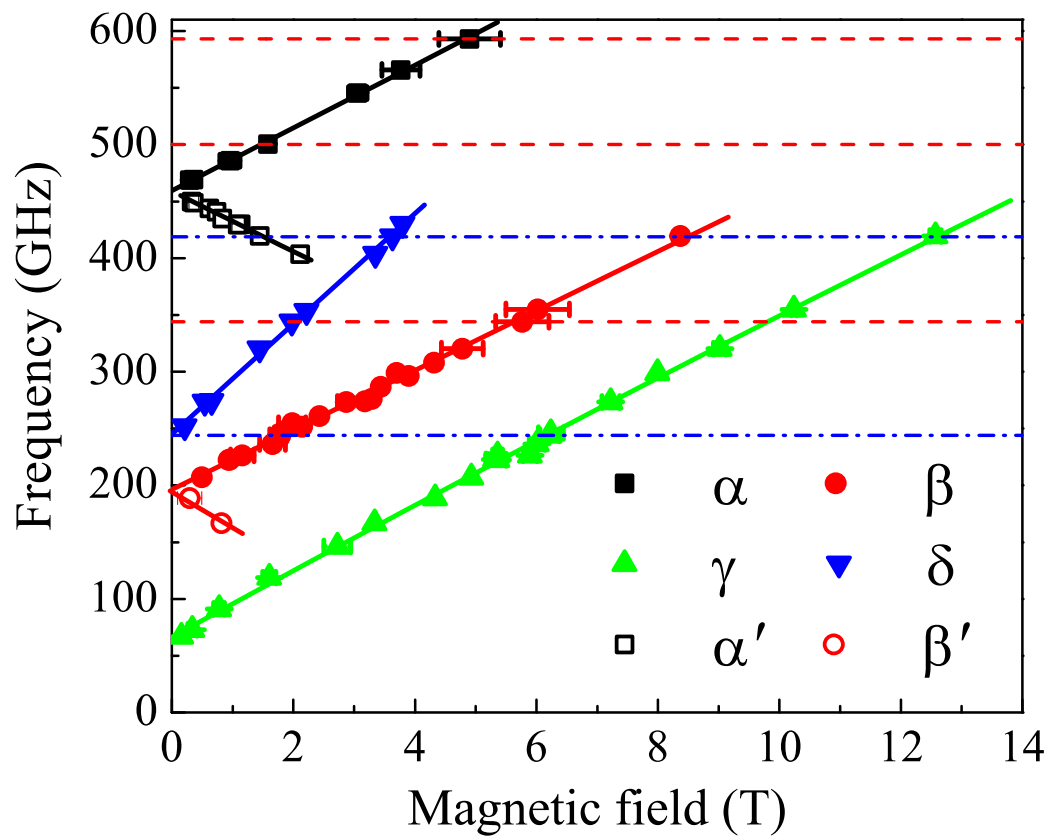


Fig. 5, Liu et al.

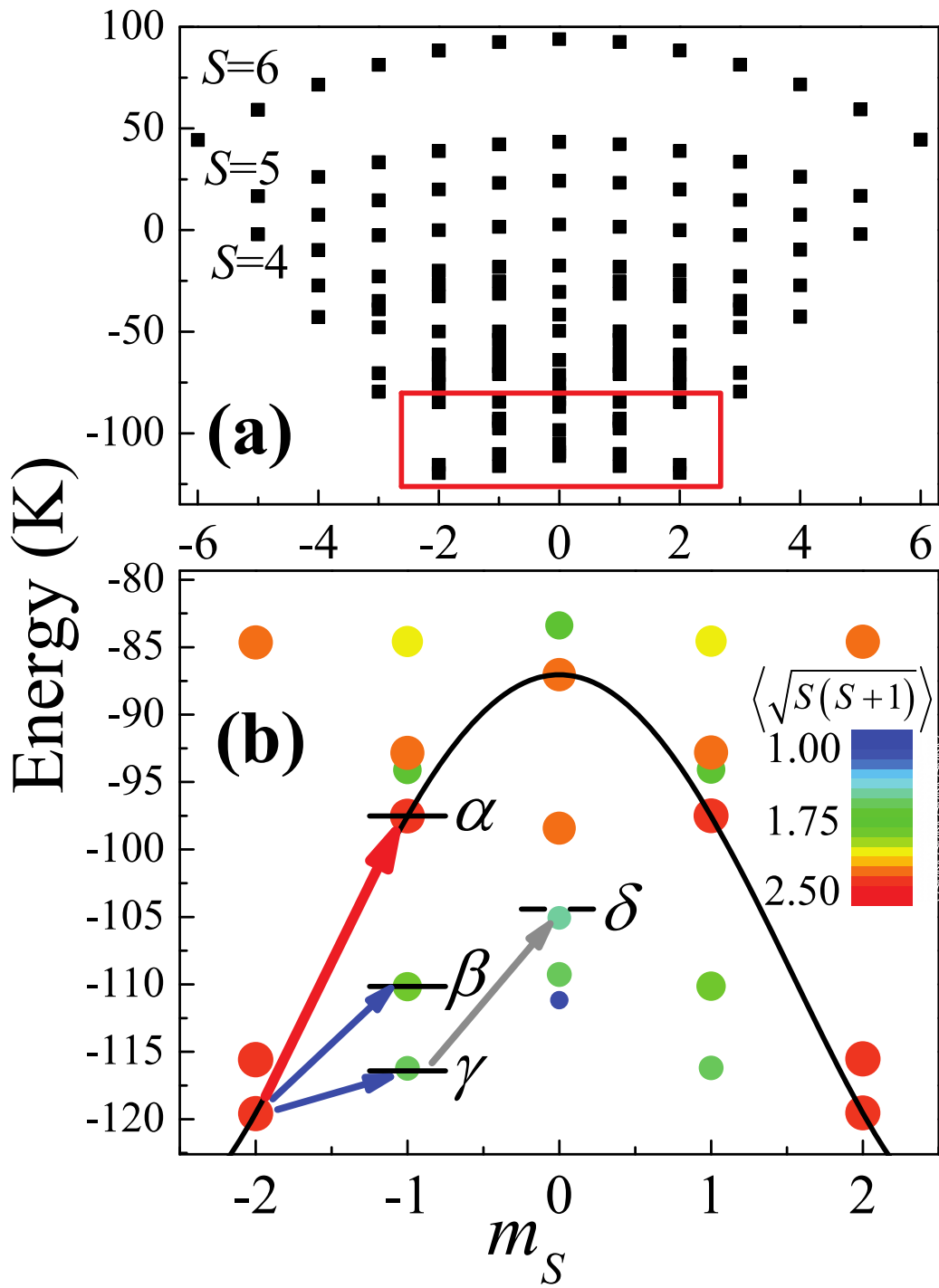


Fig. 6, Liu et al.

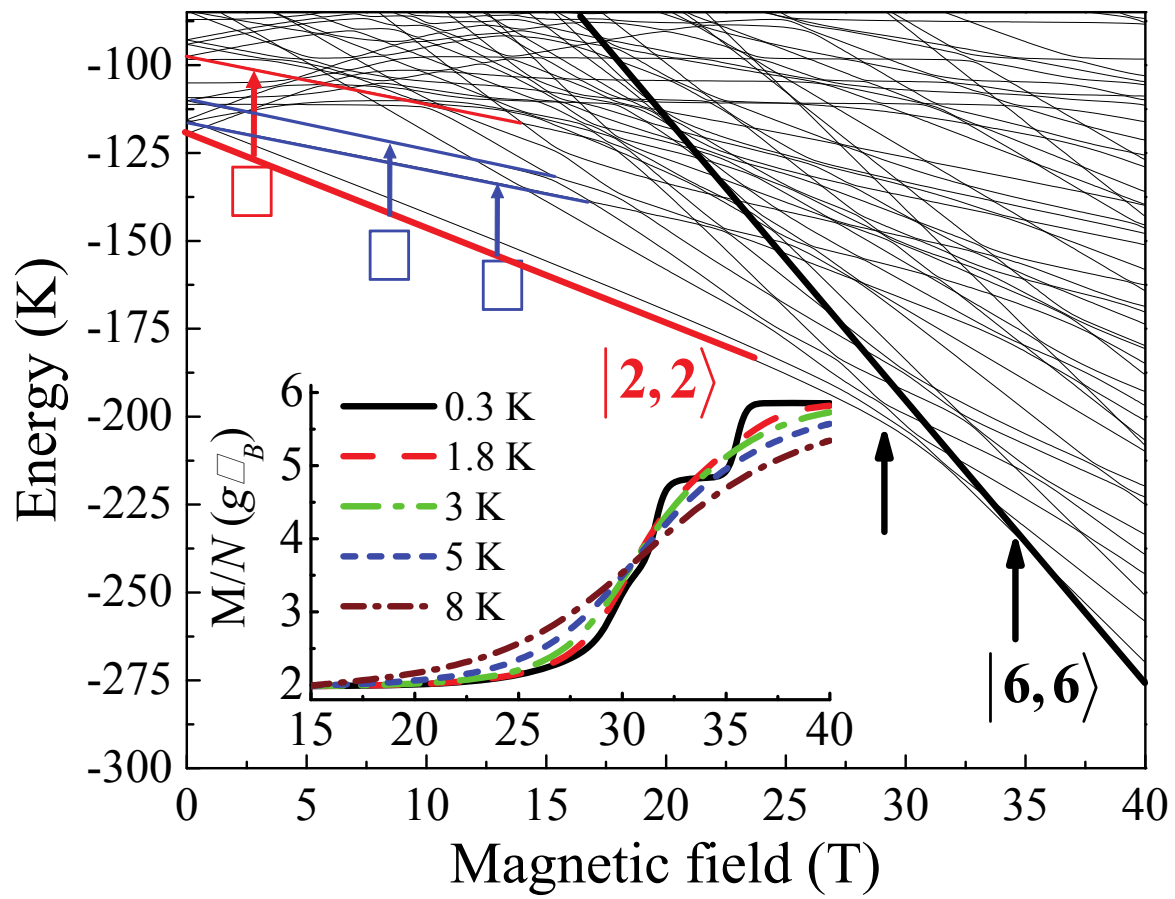


Fig. 7, Liu et al.

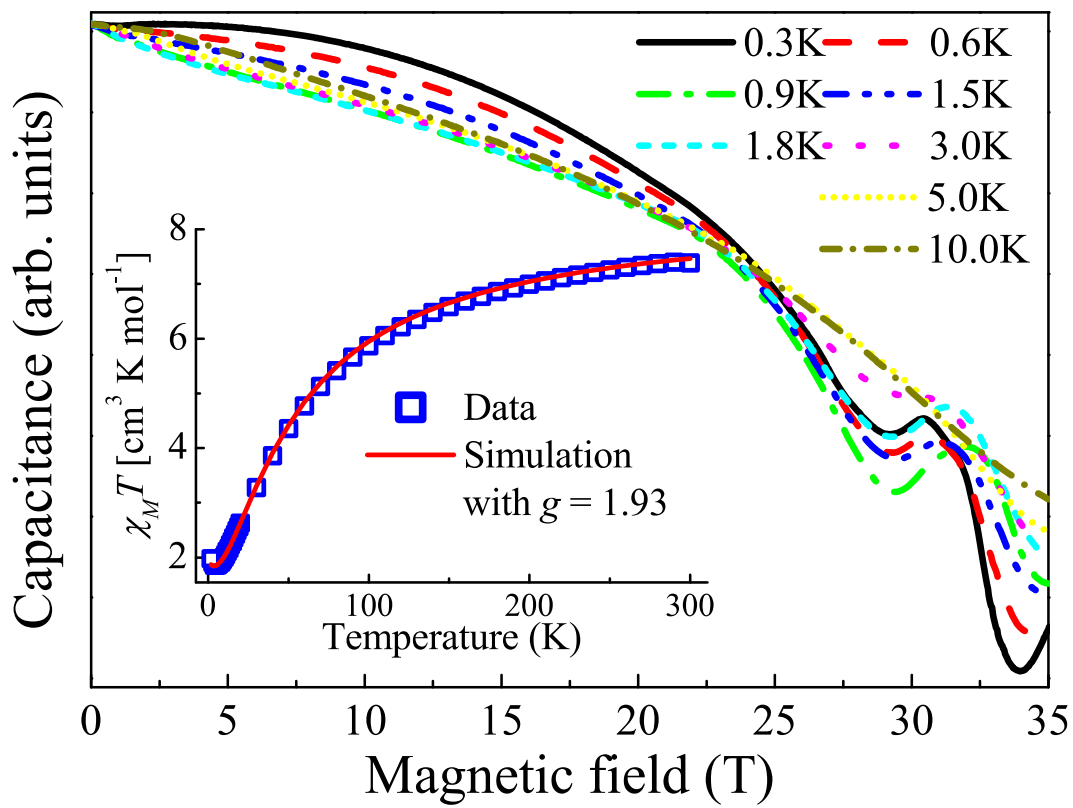


Fig. 8, Liu et al.